

MEASUREMENT AND OPTIMIZATION OF THE EMITTANCE OF A 300-ns 250-A 3.4-MeV ELECTRON BEAM*

R. W. Allison, Jr., J. W. Beal, W. L. Everette, J. R. Guggemos,
W. A. S. Lamb, R. M. Richter, W. A. Sherwood, R. L. Spoerlein,
J. Tanabe, R. E. Wright, and E. Zajec

Lawrence Radiation Laboratory
University of California
Berkeley, California

The two-dimensional emittance of the 3.4-MeV 250-A beam produced by the Astron linear induction accelerator has been measured. The measurement utilized a slit plate and a glass slide. A densitometer scan of the slit pattern formed on the glass by irradiation was analyzed and emittance contours drawn.

Substitution of a radiation-resistant Cr^{3+} -activated Al_2O_3 scintillator permitted observation of the slit pattern of each pulse by using television. This equipment allowed the induction accelerator to be tuned for minimum emittance without excessive beam loss. Ninety percent of the beam was within a phase-plane area of 0.17 cm-radian. Data on the two-dimensional phase-space density are also presented.

Introduction

In order to obtain data for the design of the transport system used in the recent electron ring experiment at LRL,¹ the two-dimensional emittance of the beam produced by the Astron linear induction accelerator² has been measured. The measurement technique used a slit plate³ and a glass slide. A densitometer scan of the pattern formed on the glass by irradiation was analyzed and emittance contours drawn. The current within each contour and the maximum density in the phase space has also been computed. A radiation-resistant $\text{Al}_2\text{O}_3(\text{Cr}^{3+})$ scintillator permitted observation of the slit pattern during each pulse by using television. This equipment allowed the induction accelerator to be tuned for minimum emittance without excessive beam transmission loss.

Experimental Setup

A sketch of the experimental equipment is shown in Fig. 1. A beam transport system with five solenoid focusing magnets was used to transport the beam from the linear induction accelerator, past the Astron experimental tank, to the diagnostic box. The total transport distance was 4.7 meters, and the acceptance of the beam line was 0.5 cm-radian.

*Work done under auspices of the U. S. Atomic Energy Commission.

Near the exit of the induction accelerator were located a beam toroid (BT1) and a set of magnetic induction position detectors ($\Delta X_1, \Delta Y_1$). Downstream from these devices four steering coils (DM1, DM2) were located, inside solenoids S2 and S3, respectively. A water-cooled aluminum target (T1) was located at the entrance of the beam diagnostic box. The diagnostic box contained a beam toroid (BT2), a slit plate with 10 slits, an aluminum oxide scintillator, and a glass slide holder. The slits, scintillator, and glass slide were mounted on motor-driven probes. The slide probe retracted into an air lock, which allowed removal of the glass slide after each irradiation. The diagnostic box had a view window through which the scintillator was viewed by using a Vidicon. The slit plate dimensions are sketched in Fig. 1A. Each slit was 0.38 mm wide, the slit separation was 6.25 mm. The slit plate was constructed of carbon and was 1.25 cm thick. The spacing between the slit and slide was 14.5 cm. A deep Faraday cup terminated the beam line. This cup had an aperture of 2.54 cm and was 47 cm deep.

Experimental Procedure

Before exposing each glass plate, the induction accelerator and transport system were tuned for minimum emittance at the desired current. This was done in the following way:

- T1 was inserted in the beam and the induction accelerator tuned for optimum beam transmission and minimum position sweep at BT1 and $\Delta X_1, \Delta Y_1$.
- T1 was then removed and the beam maximized on BT2 and the Faraday cup by tuning the beam transport system.
- The emittance slits and scintillator were then inserted in the beam and the accelerator and transport system fine-tuned for minimum emittance by observing the slit pattern on each pulse.

Typically the beam transmission from the accelerator electron gun to BT1 was 80%; at BT2, 70 to 75% was usually achieved.

The exposure of the glass slide was made by inserting T1, retracting the scintillator, and inserting the glass slide; T1 was then removed

and seven pulses of beam were received by the slide. At the end of the exposure the slide was removed from the vacuum through the air lock. Use of the technique described above permitted exposure of each slide without shutdown of the accelerator, and thus ensured that the measurement took place while the output beam was stable.

Measurements were made over a current range of 100 to 250 A at BT2. The beam energy was 3.4 MeV, the energy spread about $\pm 1.5\%$. The beam pulse (with the exception of one measurement) was 300 ns. The accelerator was operated at a PRF of 2 pulses/s. The accelerator core voltages were held constant at 28 kV. The gun cores were operated at 26 kV to ensure maximum stability. (This voltage limited the maximum current obtained.)

A typical slit pattern is shown in Fig. 2.

Data Reduction

The pattern formed on each slide was scanned by use of a densitometer. The effective slit width in the scan direction was 18μ , the slit height was 1.5 cm. Background from x rays and low-energy electrons was minimized by adjusting the densitometer zero. Two of the density scans are shown in Fig. 3a,b. At the i th slit the profile peak represents the phase-space density $\rho(X_1 X')$ at $X' = 0$. The width of the i th profile represents the divergence of the beam at X_1 . If ρ_0 is the peak density (the maximum of the envelope about all the profiles) then a line of constant relative density, $E_j = \rho/\rho_0$, is represented by a horizontal line. The divergence of the beam at the i th slit is computed from the intercept of this line with the i th density profile: $\theta = (X_r - X_i - \frac{w}{2})/L$, where L = separation of slit and slide, w = slit width, X_1 = slit location, and X_r = intercept location. (We have taken the edge of the first slit as the coordinate system zero.) The beam current within an emittance contour was obtained from $I_c = I_t A_c/A_t$, where A_t is the total area of the density profiles and A_c is the total profile area within the divergence intercepts. This area is shaded in Fig. 3a,b. The total current, I_t , was taken to be the current read on BT2. Divergences and currents within a constant density were computed for $E_j = 0.1, 0.3, 0.5, 0.8, \text{ and } 0.9$.

The emittance contours that correspond to the density profiles of Fig. 3a,b are shown in Fig. 4a,b. Each contour was formed by connecting adjacent (X, X') points with straight lines. For convenience the coordinate system used in reducing the densitometer scans was transformed to a coordinate system in (X, X') with a zero which was the center of gravity of $E_j = 0.9$. In all the data the emittance numbers are the actual phase-plane area in cm-radians, at 3.4 MeV.

For comparison of different exposures we have plotted (Fig. 5) the current within each contour against the two-dimensional phase-space area within each contour. In addition, the maximum

density of the phase space was computed from

$$\rho_0 = I_t / \int (\rho/\rho_0) dx dx' = I_t / \int (\rho/\rho_0) dA,$$

where the integral in the denominator was numerically evaluated from plots of ϵ_j vs the two-dimensional emittance A . The results of this computation are plotted in Fig. 6.

An examination of Figs. 3 and 4 indicates that changes in beam divergence are readily determined. Low-energy electrons scattered from the slits apparently do not seriously affect the measurement. We did not adjust the divergence for space-charge effects, since only 5 A total beam is transmitted by the slits, and this produces a negligible change in the beam divergence at 3.4 MeV.

Experimental Results

An examination of Fig. 5 indicates that as the total beam current increases more current appears at larger emittances. This effect is especially apparent when the 200- and 250-A runs are compared. In addition the peak density in phase space (Fig. 6) rises to a maximum at 190 A and then flattens out at higher current. At 190 A 90% of the current is centered within a phase-plane area of 0.17 cm-radian, 50% of the current within an area of 0.037 cm-radian. At 250 A the areas are 0.215 and 0.049 cm-radian respectively. The maximum phase-space density at 190 A is 2990 A/cm-radian, at 250 A it is 2669 A/cm-radian. This saturation of the central core of the beam indicates that for this particular electron gun a limit has been reached, and that any additional increase in output current results in an increase in the beam emittance.

An emittance measurement of a 20-ns portion of the 300-ns beam pulse has been made and also plotted in Figs. 5 and 6. It is obvious that this short beam pulse has a higher phase-space density ($\rho_0 = 3860$ A/cm-radian) than that of the 300-ns pulse. Thus it is possible that the limit reached in the long-pulse-beam phase-space density is due to some time-dependent parameter such as emission variation or beam sweeping due to accelerator voltage variations.

We have taken the 190-A measurement and, using an impulse approximation for space charge, obtained the location of the apparent 3.4-MeV object produced by the induction accelerator. It is located 31 cm inside the last accelerating section, and has a beam width of 2.9 cm and a divergence of ± 0.038 radian.

References

1. R. W. Allison et al., UCRL-18498, 1 Oct. 1968, to be published in Proceedings of National Accelerator Conference, Moscow, USSR, Oct. 1968.
D. Keefe et al., UCRL-18671., Dec. 1968.

2. J. W. Beal, The Astron Linear Accelerator, in Proceedings of the 1968 Linear Accelerator Conference, P713, 1968.
3. B. Vosicki, in Proceedings of the 1966 Linear Accelerator Conference, 344, 1966.
H. Wroe, Nucl. Instr. Methods 58, 213 (1968).

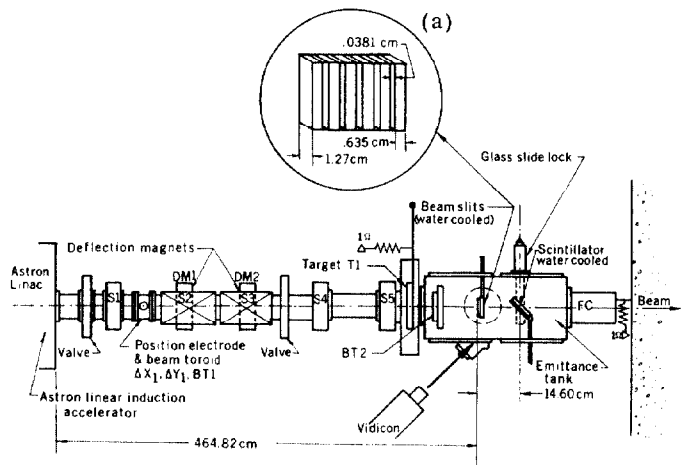


Fig. 1. Experimental setup, showing beam line and diagnostic equipment.



Fig. 2. Photograph of irradiated slide (Figures 3B and 4B are obtained from this slide).

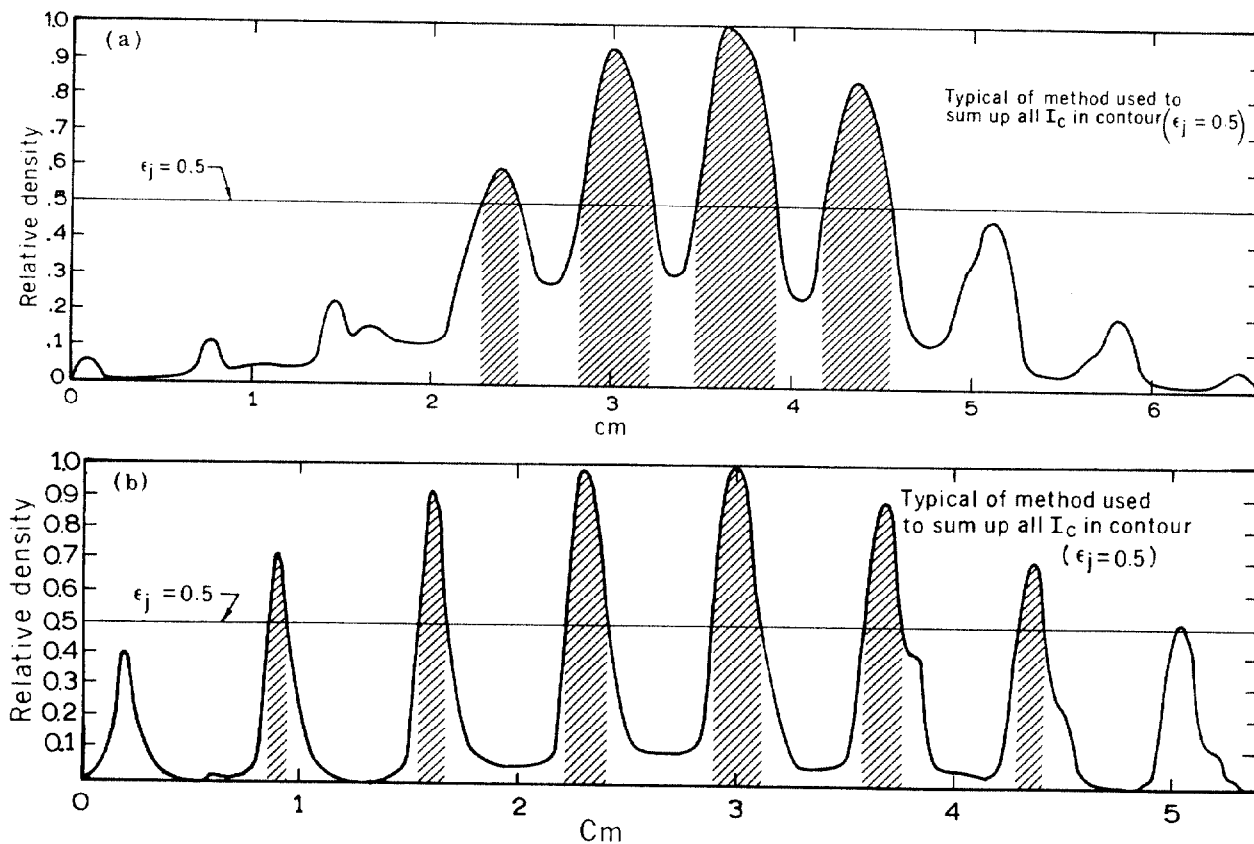


Fig. 3. Density scan of (a) 200-A, (b) 190-A, 3.4-MeV beam.

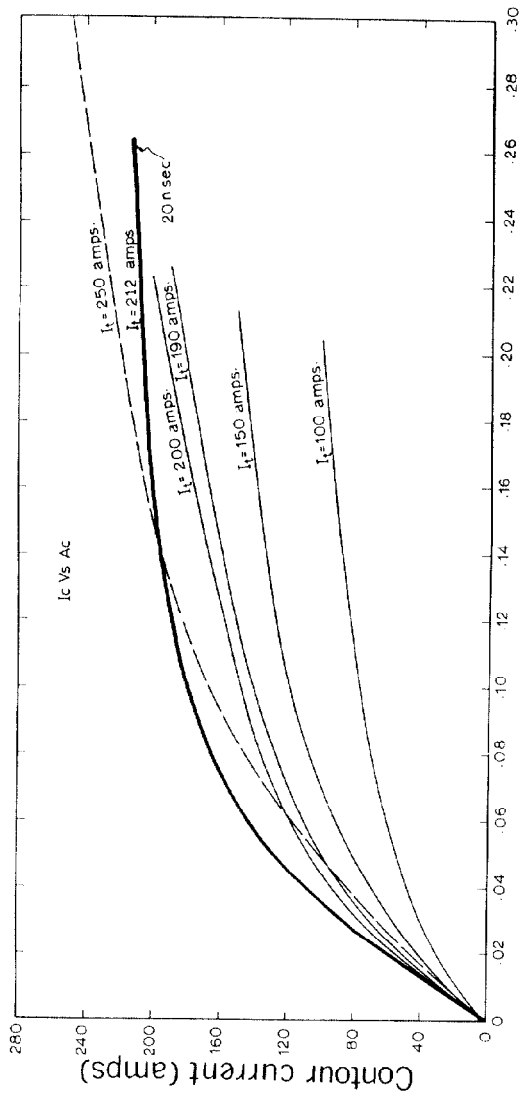


Fig. 5. I_c (current within a contour) as a function of the two-dimensional phase-space area.

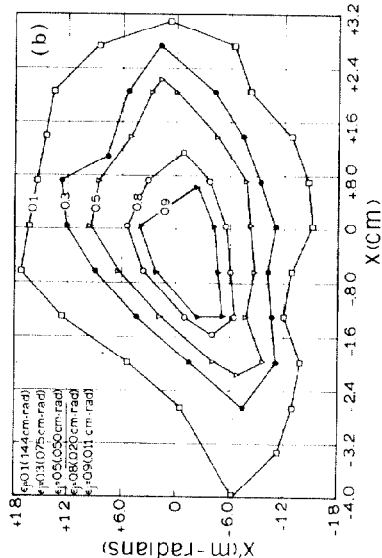
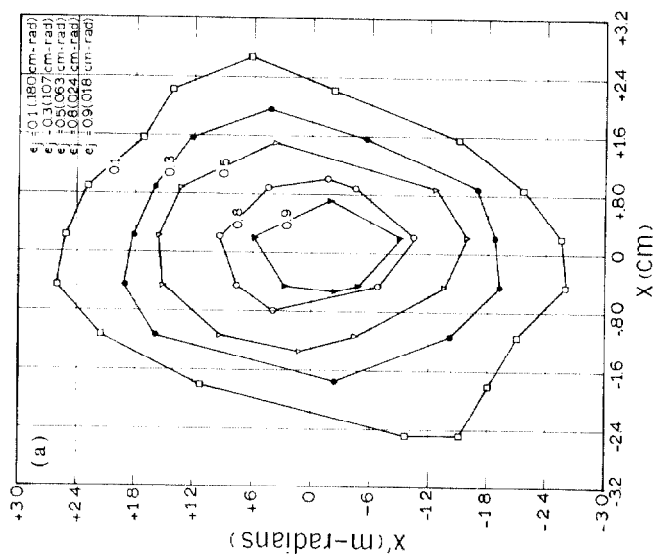


Fig. 4. (a) 200-A, (b) 190-A emittance contours.

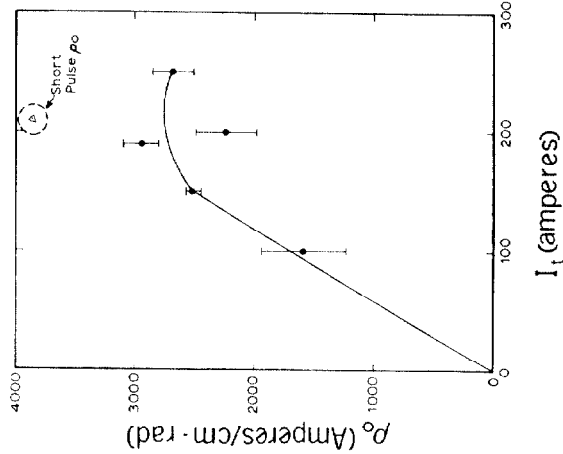


Fig. 6. Plot of the maximum phase space density ρ_0 as a function of the beam current, I_t .